The Journal of Physiology

Inner retinal inhibition shapes the receptive field of retinal ganglion cells in primate

D. A. Protti[1,2], S. Di Marco[1,2], J. Y. Huang[3], C. R. Vonhoff[1,2], V. Nguyen[1,2] and S. G. Solomon[1,2,4,5]

[1] *Discipline of Physiology,* [2] *Bosch Institute, and* [3] *Discipline of Biomedical Science, The University of Sydney, NSW 2006, Australia*
[4] *ARC Centre of Excellence in Vision Science, and* [5] *Cognitive, Perceptual and Brain Sciences, University College London, London, UK*

Key points

- The receptive field of most retinal ganglion cells consists of an excitatory centre and an inhibitory surround.
- In retinal ganglion cells of non-primates the receptive field surround is provided by lateral inhibition in both the outer and the inner retinal synaptic layers.
- We use whole cell recording methods to establish the spatial organisation of excitatory and inhibitory synaptic inputs onto ganglion cells in primate retina.
- We confirm centre–surround organisation in the excitatory inputs to ganglion cells, and show further that inhibitory inputs can also show centre–surround organisation.
- We show that lateral inhibition in the inner retina shapes the spatial profile of both excitatory and inhibitory synaptic inputs onto ganglion cells.
- Dynamic clamp experiments provide evidence that reduction of inner retinal inhibition reduces spatial tuning in ganglion cell output.
- These results show that lateral inhibition in the inner retina of primate shapes the analysis of spatial form and contrast.

Abstract The centre–surround organisation of receptive fields is a feature of most retinal ganglion cells (RGCs) and is critical for spatial discrimination and contrast detection. Although lateral inhibitory processes are known to be important in generating the receptive field surround, the contribution of each of the two synaptic layers in the primate retina remains unclear. Here we studied the spatial organisation of excitatory and inhibitory synaptic inputs onto ON and OFF ganglion cells in the primate retina. All RGCs showed an increase in excitation in response to stimulus of preferred polarity. Inhibition onto RGCs comprised two types of responses to preferred polarity: some RGCs showed an increase in inhibition whilst others showed removal of tonic inhibition. Excitatory inputs were strongly spatially tuned but inhibitory inputs showed more variable organisation: in some neurons they were as strongly tuned as excitation, and in others inhibitory inputs showed no spatial tuning. We targeted one source of inner retinal inhibition by functionally ablating spiking amacrine cells with bath application of tetrodotoxin (TTX). TTX significantly reduced the spatial tuning of excitatory inputs. In addition, TTX reduced inhibition onto those RGCs where a stimulus of preferred polarity increased inhibition. Reconstruction of the spatial tuning properties by somatic injection of excitatory and inhibitory synaptic conductances verified that TTX-mediated inhibition onto bipolar cells increases the strength of the surround in RGC spiking output. These results indicate that in the primate retina inhibitory mechanisms in the inner plexiform layer sharpen the spatial tuning of ganglion cells.

© 2013 The Authors. *The Journal of Physiology* published by John Wiley & Sons Ltd on behalf of The Physiological Society.
DOI: 10.1113/jphysiol.2013.257352
This is an open access article under the terms of the Creative Commons Attribution License, which permits use, distribution and reproduction in any medium, provided the original work is properly cited.

Downloaded from J Physiol (jp.physoc.org) at UCL Library Services on September 25, 2014

(Received 22 April 2013; accepted after revision 13 September 2013; first published online 16 September 2013)
Corresponding author D. A. Protti: Anderson Stuart Bldg (F13), The University of Sydney, NSW 2006, Australia. Email: dario.protti@sydney.edu.au

Abbreviations EAAT, excitatory amino acid transporter; IPL, inner plexiform layer; OPL, outer plexiform layer; RGC, retinal ganglion cell; SI, surround index; TTX, tetrodotoxin.

Introduction

Centre–surround organisation is a fundamental property of the receptive field of most retinal ganglion cells (RGCs) critical for extraction of visual features. In these neurons an appropriate stimulus presented to the smaller 'centre' increases the discharge rate, while stimulation of the larger, concentric 'surround' decreases the discharge rate. The centre response is mostly driven by excitatory input from bipolar cells but the neural circuits underlying the surround are less clear. In the vertebrate retina, there is evidence for a role of surround inhibition at the level of both outer and inner plexiform layers (Wässle, 2004; Eggers & Lukasiewicz, 2010*b*).

In the outer retina negative feedback from horizontal cells modulates the output of photoreceptors (VanLeeuwen *et al.* 2009) and may also provide inhibitory input to bipolar cells (Werblin, 1974). The receptive field of the bipolar cell therefore usually shows centre–surround organisation, and RGCs will inherit this. Inhibitory feedback in the outer plexiform layer (OPL) may be mediated via a shift in the voltage dependence of calcium currents in cones, hemichannels and/or pH modulating photoreceptor transmitter release and via GABA receptors on bipolar cell dendrites (see Thoreson & Mangel, 2012 for review).

In addition, inhibitory processes in the inner plexiform layer (IPL) have been shown to contribute to the spatial profile of ganglion cell receptive fields via two distinct mechanisms: inhibitory synapses onto bipolar cell terminals (presynaptic inhibition) and inhibitory synapses onto the RGCs themselves (direct inhibition). Stimulation of the receptive field surround recruits GABA-mediated inhibition onto bipolar cell terminals, which curtails neurotransmitter release (Flores-Herr *et al.* 2001; Eggers *et al.* 2007; Eggers & Lukasiewicz, 2010*b*). Direct inhibitory inputs onto RGCs are drawn from wide-field and small-field amacrine cells (Flores-Herr *et al.* 2001; Chen *et al.* 2010; Farrow *et al.* 2013).

While substantial work in other species suggests that the receptive field surround of RGCs is built in both the OPL and the IPL, the contribution of each network to the receptive field surround of primate ganglion cells remains unknown. In macaque retina, the surround of parasol cells seems to be largely generated in the outer retina where it is mediated by hemichannels (McMahon *et al.* 2004) and pH-mediated feedback (Davenport *et al.* 2008) onto photoreceptors. These studies showed that neither application of GABA receptor blockers nor tetrodotoxin (TTX), which targets spiking amacrine cells, modify the area–response function of RGCs. Nevertheless, other studies show that both parasol and midget RGCs in the macaque retina receive strong inhibitory inputs from amacrine cells (Crook *et al.* 2009, 2011), thus reigniting the question of whether lateral inhibition in the primate IPL helps sculpt the spatial profile of RGCs.

To determine whether inhibitory mechanisms in the IPL are involved in shaping the spatial profile of RGCs, we characterised the spatial organisation of the light-evoked synaptic inputs onto ON- and OFF-RGCs of the marmoset, a diurnal New World primate. The structural and functional properties of the retina and subcortical visual pathways of the marmoset are very similar to those of Old World primates, including macaques (Ghosh *et al.* 1996; Kremers & Weiss, 1997; Solomon *et al.* 1999).

Methods

Ethical approval

Procedures were approved by the University of Sydney Animal Ethics Committee, and conform to both the Society for Neuroscience and the National Health and Medical Research Council of Australia policies on the use of animals in research. The authors have read, and the experiments comply with, the policies and regulations of *The Journal of Physiology* given by Drummond (2009).

General

Recordings were made from retinal tissue from 19 adult marmosets (*Callithrix jacchus*, 17 males) obtained at the end of unrelated neurophysiological recording experiments (Camp *et al.* 2009, 2011; Solomon *et al.* 2010). Animals were dark-adapted for at least 40 min before the eyes were enucleated under dim red light. During eye removal a surgical level of anaesthesia was provided by inhalation of isoflurane (3–4%) in a mixture of 70% NO_2 and 30% carbogen (5% CO_2/95% O_2), delivered by artificial respiration through a tracheal cannula. After eye removal the animal was immediately killed by intravenous injection of 500 mg kg^{-1} sodium pentobarbitone (Lethobarb; Verbac Australia, Milperra,

© 2013 The Authors. *The Journal of Physiology* published by John Wiley & Sons Ltd on behalf of The Physiological Society.

Downloaded from J Physiol (jp.physoc.org) at UCL Library Services on September 25, 2014

NSW, Australia). The eyes were cut open around the cornea, the lens and vitreous were removed, and the eyecups consisting of sclera and retina were transferred to a beaker containing carboxygenated Ames medium in a light-tight box where the retina was dark-adapted for at least 1 h. The remainder of the procedures were carried out under infrared illumination. After dark-adapting, the eyecup was transferred to a Petri dish containing carboxygenated Ames medium, a quadrant was cut from the eyecup and the remaining tissue placed back in the light-tight box. From this quadrant the neural retina was detached from the pigment epithelium, placed photoreceptor side down in a recording chamber and transferred to the microscope stage, where it was continuously perfused with carboxygenated Ames medium heated to 35°C. Cells were viewed on a video monitor coupled to a CCD camera mounted on an Axioskop microscope (Carl Zeiss, Göttingen, Germany) illuminated with infrared light.

Visual stimuli

Achromatic stimuli were displayed via a DLP projector (Infocus 120, Portland, OR, USA; refresh rate 60 Hz) through the microscope optics and focused onto the photoreceptors. Stimuli consisted of uniform spots (0.5 s) of different diameters (varying from 30 to 1200/1400 μm) centred on the soma. The display was held at the mean luminance, which was 0.025 cd m^{-2}. ON and OFF responses were elicited by an increment or a decrement in intensity, respectively, from the mean luminance. For some ON ganglion cells, the mean luminance was reduced. Stimuli were generated using EXPO (P. Lennie, University of Rochester, Rochester, NY, USA).

Electrophysiological recordings

Voltage-clamp. Cell-attached and whole-cell recordings were obtained from RGCs in whole-mount retinas in voltage-clamp mode using an EPC10 patch-clamp amplifier (HEKA Elektronik, Lambrecht, Germany). Patch electrodes were filled with an intracellular solution containing (in mM): 110 Caesium Methanesulphonate, 5 tetrabutylammonium, 20 Hepes, 10 EGTA, 4.6 $MgCl_2$, 4 Na-ATP, 0.5 Na-GTP, 20 creatine phosphate and 250 U ml^{-1} creatine phosphokinase. Voltage-gated sodium currents were blocked by adding 5 mM QX-314 to the intracellular solution. Lucifer yellow (2%) was added to the intracellular solutions for cell identification. Ames medium was perfused at 3 ml min^{-1}. A liquid junction potential of −15 mV was subtracted from voltage values offline. Patch pipettes of 6–8 MΩ were used; series resistance usually ranged between 25 and 35 MΩ and was left uncompensated. The chloride reversal potential [ECl^-] for these solutions was calculated to be approximately −65 mV.

Dynamic clamp. Dynamic-clamp recordings enable the injection of excitatory and inhibitory synaptic conductances. RGCs were patched in whole-cell configuration and membrane potential was monitored in fast current-clamp mode. Signals were acquired with an EPC8 patch-clamp amplifier (HEKA Elektronik) and digitised at 40 kHz with an FPGA card (National Instruments, Austin, TX, USA). Patch electrodes were filled with a potassium-based intracellular solution containing (in mM): 140 potassium gluconate, 4.6 $MgCl_2$, 10 EGTA, 10 Hepes, 4 Na-ATP and 0.4 Na-GTP. The current injected in dynamic-clamp experiments was computed from the measured membrane potential, the excitatory and inhibitory synaptic conductance waveforms, and the reversal potential of excitatory (0 mV) and inhibitory (–75 mV) inputs using the custom written software NeuroAkuma (kindly provided by Dr Klaus Stiefel, University of Western Sydney, Australia). The calculated current was fed back into the cell using the same FPGA via the EPC8 amplifier at 40 kHz. The synaptic conductance waveforms used in dynamic clamp experiments corresponded to one example OFF cell in which there was size tuning of excitation and increase in inhibition in response to preferred contrast stimulation. Conductance waveforms measured for varying spot sizes in control conditions and in the presence of TTX were injected into different ganglion cell types.

Analyses

Conductance analysis. Light-evoked synaptic conductances were calculated following a modified version of previously described methods (Borg-Graham, 2001; Taylor & Vaney, 2002; Di Marco *et al.* 2009) in terms of the magnitude of G_{exc} and G_{inh}, as follows. Light-evoked synaptic currents were elicited by displaying spots of varying diameters (or annuli) at holding potentials ranging from −105 to +45 mV every 10 mV. As currents contained a residual potassium current with a time-dependent inactivation component in response to depolarising potentials over −10 mV, a linear fit was calculated between 200 ms before and after the light response, which was masked for the fit, and then subtracted from the currents. The mean amplitude of the last 100 ms of the voltage step was then added back to the currents. The mean amplitude of 10 ms segments of light-evoked synaptic currents with respect to baseline (current amplitude averaged for 200 ms before stimulus presentation) was used to plot current–voltage curves, from which the reversal potential (E_{rev}) and total conductance (G_T) were estimated from the crossing at

© 2013 The Authors. *The Journal of Physiology* published by John Wiley & Sons Ltd on behalf of The Physiological Society.

Downloaded from J Physiol (jp.physoc.org) at UCL Library Services on September 25, 2014

current 0 pA and the slope of a linear fit of the *I–V* relation, respectively. Excitatory and inhibitory synaptic conductances (G_{exc} and G_{inh}, respectively) were estimated from:

$$G_{exc}(t) = \frac{G_T(t) \times (E_{rev}(t) - E_{inh})}{E_{exc} - E_{inh}},$$

$$G_{inh}(t) = \frac{G_T(t) \times (E_{rev}(t) - E_{exc})}{E_{inh} - E_{exc}}$$

in which E_{exc}, the reversal potential of excitatory currents, was considered to be 0 mV, and E_{inh}, the reversal potential of chloride, was estimated to be −65 mV.

Spikes were recorded in loose cell-attached extracellular recordings in voltage-clamp mode and detected using an offline routine to detect the location of maxima by calculating the smooth first and second derivative of the current signal and comparing it to a threshold. Spike count in the absence of visual stimulus (spontaneous activity) was subtracted before analysis. We isolated excitatory and inhibitory currents by recording in voltage-clamp mode at the reversal potential of inhibitory and excitatory currents (−60 and 0 mV), respectively. Area–response functions for excitatory and inhibitory inputs were estimated from the area of the inward and outward currents, respectively, by integrating the signal (i.e. light evoked charge transfer over the duration of stimulus presentation). From the area–response function of individual cells, we determined the spot size that produced the strongest response (measured as spikes, current or conductance) and defined it as optimal spot size. Response strength and spot sizes were normalised to optimal spot size to allow comparisons of the receptive field properties of different cell types recorded at different eccentricities. This procedure was previously used to characterise the receptive field surround of bipolar cells (Eggers & Lukasiewicz, 2010*a*) and ganglion cells (Sagdullaev & McCall, 2005).

Difference-of-Gaussians model. Area–response curves were characterised by finding the best predictions of a difference-of-Gaussians model (Rodieck, 1965; Enroth-Cugell & Robson, 1966). The model has four parameters – the integrated volume and width (standard deviation) of an excitatory centre (K_c and R_c) Gaussian, and the integrated volume and width of a concentric, inhibitory surround (K_s and R_s) Gaussian. The size of the surround was constrained to be larger than that of the centre. For spike count, charge transfer or integral of conductance we found the combination of parameters that best predicted response (in a least-squares sense), using the function *lsqcurvefit* in the Matlab environment or Levenberg–Marquardt least-squares method in Igor. To quantify the strength of the 'surround' component of the receptive field we calculated a surround index (SI), $SI = [1 - (R_{Max}/R_{Peak})] \times 100$. R_{Max} is the response elicited with the largest spot size and R_{Peak} is the response at the optimal size. An index of 100 indicates that making the stimulus large abolished response completely and an index of 0 indicates that increasing the size of the stimulus did not reduce response.

Immunostaining, microscopy and estimation of dendritic field size. At the end of the recordings, retinae were fixed in paraformaldehyde (4% in PBS) for 30 min and then washed in PBS 0.2 M three times for 10 min each. The tissue was then incubated for 5 days in a 1:10,000 primary antibody solution (rabbit polyclonal anti-LY antibody, Invitrogen, Carlsbad, CA, USA) containing 0.5% Triton X-100, 0.1% bovine serum albumin (BSA) and 0.05% sodium azide in 0.1 M PBS. The tissue was subsequently washed for a full day in 0.1 M PBS and incubated overnight in 1:500 anti-rabbit antibody IgG conjugated with Alexa 594 (Invitrogen), 0.5% Triton X-100 and 0.1% BSA in PBS. Whole mounts were washed for a full day before mounting for confocal microscopy. Immunofluorescence images of RGCs were acquired on a laser-scanning confocal microscope (LSM 510, Carl Zeiss). Serial sections in the z plane were acquired and subsequently stacked to morphologically reconstruct the cells. We drew a convex polygon connecting the most distal tips of the dendrites of the Lucifer Yellow-filled cells and measured its area using AxioVisionLE. Dendritic field diameter is expressed as the diameter of a circle with an equivalent area to that of the polygon.

Statistics. Values in the text and figures represent mean ± standard error of the mean (SEM). Statistical significance between two groups was calculated by paired Student's *t* test unless otherwise stated. The criterion for statistical significance was $P \leq 0.05$.

Results

We report observations from extracellular and whole-cell recordings made *in vitro* from whole-mount preparations of the marmoset retina. The available measurements include extracellular recordings made from 28 RCGs in 18 retinal whole mounts; whole-cell recordings were made from 10 of these, and from 28 more RGCs obtained from 19 other whole mounts. We include only cells that generated action potentials, or showed large voltage-activated sodium currents during the initial phase of whole-cell recording, so our sample is not likely to include amacrine cells. Recordings were made only from neurons with large soma (>15 μm diameter) located in the ganglion cell layer at a minimum distance of 2 mm and no further than 10 mm from the fovea. At this range of eccentricities soma sizes of the most abundant RGC types,

© 2013 The Authors. *The Journal of Physiology* published by John Wiley & Sons Ltd on behalf of The Physiological Society.

Downloaded from J Physiol (jp.physoc.org) at UCL Library Services on September 25, 2014

midget and parasol, are 15 μm or more (Ghosh *et al.* 1996). Morphological reconstruction was possible only in a few cases, so in the following we do not attempt to characterise how functional properties vary with morphological class. Our aim is to test whether bipolar cell output in the primate retina is modulated by inhibitory processes in the IPL and whether RGCs, like those in other mammals, draw inhibition from amacrine cells to help shape the receptive field.

Spatial summation in spike response of marmoset retinal ganglion cells

Figure 1*A* and *B* shows the extracellular measurements from a representative ON-RGC. Figure 1*A* shows action potentials during presentation of a spot of light at each of three different sizes. Figure 1*B* shows the spike count over the duration of the stimulus (0.5 s), for these stimuli and for additional stimuli of intermediate sizes. Most RGCs showed spontaneous activity (mean frequency $= 2.5 \pm 0.7$ Hz, $n = 28$), which was removed before analysis. The area–response function of this cell shows classical centre–surround receptive field organisation: response strength increases with spot diameter up to an optimal size and rolls off for larger sizes. The dashed line in Fig. 1*B* shows the best prediction of a difference-of-Gaussians model of the receptive field (see Methods). For this cell the centre radius was 92 μm and the surround radius was 310 μm. Figure 1*C* shows the morphology of the same ON-RGC, which resembles a parasol ganglion cell located relatively centrally. The dendritic field diameter was 106 μm.

Figure 1*D* shows average area–response functions for the populations of ON and OFF-RGCs we recorded from. To generate these average curves we normalised response amplitude and size of each cell to the preferred stimulus before averaging. Figure 1*D* confirms that receptive field surrounds are prominent in both ON and OFF-RGCs in marmoset retina. To quantify the strength of receptive field

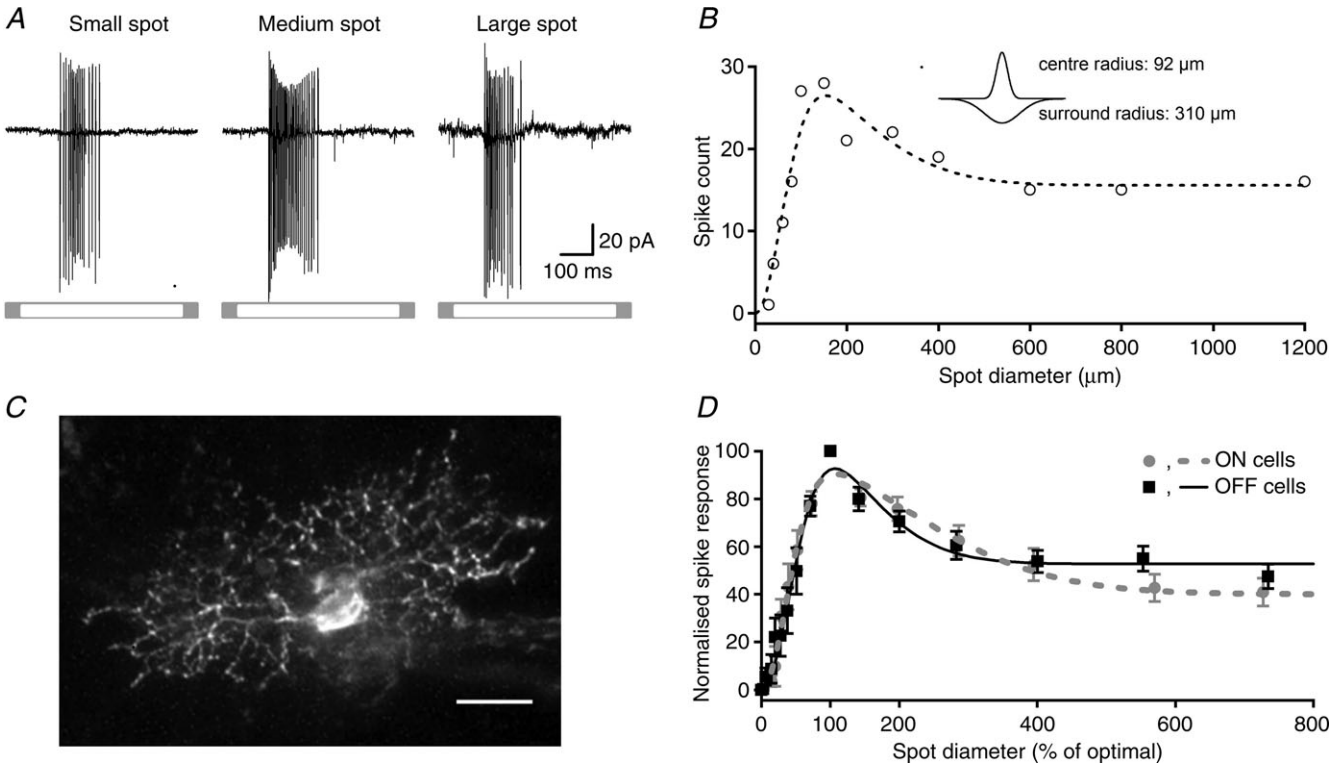

Figure 1. Receptive fields of marmoset retinal ganglion cells show classical centre–surround organisation
A, spike response, recorded in loose-patch configuration, of an ON-cell to circular spots of small, medium and large diameter (stimulus duration 500 ms). *B*, area–response function for spike count (open symbols) for the cell in *A*. Dashed line shows the best predictions of a difference-of-Gaussians of the receptive field, with the following parameters: $K_c = 32 \pm 6$ spikes, $R_c = 92.3 \pm 14$ μm, $K_s = 16.4 \pm 6$ spikes, $R_s = 310 \pm 20$ μm, SI = 53%. Inset shows a schematic of the receptive field profile generated by those parameters. *C*, confocal stack of the cell in *A* and *B*, which was filled with Lucifer Yellow during the recording. Scale bar = 20 μm. *D*, average area–response functions of spike response for 11 ON- and 16 OFF-RGCs. For each cell, stimulus size and response amplitude were normalised to optimal spot size and maximum response, before averaging. Difference-of-Gaussian functions were fitted to the average of the normalised area–response functions. Error bars show ±1 SEM.

© 2013 The Authors. *The Journal of Physiology* published by John Wiley & Sons Ltd on behalf of The Physiological Society.

Downloaded from J Physiol (jp.physoc.org) at UCL Library Services on September 25, 2014

surround across the population of neurons we calculated SI, the reduction in peak response brought about by a large field (see Methods). A value of 0 indicates no reduction of response in large sizes; a value of 100 indicates response was abolished by presentation of a large spot. For ON-RGCs this index was $59 \pm 6\%$ ($n = 12$); among OFF-RGCs it was $50 \pm 5\%$ ($n = 16$). Overall, large fields reduced peak response in 26/28 neurons. From the fits to difference-of-Gaussians functions we calculated the ratio of the surround to centre radius and the ratio of surround to centre volume. For ON-RGCs the surround was 5.5 ± 0.77 times the size of the centre and its volume was 0.6 ± 0.08 times that of the centre. For OFF-RGCs these values were 2.7 ± 0.72 and 0.57 ± 0.2. We calculated the first derivative (slope) of the difference-of-Gaussian function at the maximum spot size tested (1200 μm) for each cell as a measure of the rate of change in response at that size. The mean slope was -0.001 ± 0.0003 (range -0.006 to 0, $n = 28$), indicating that further expansion in spot diameter would produce little change in response. For example, the model predicts that an increase in size from 1200 to 1300 μm, a 17% increase in area, would lead to a 0.1% change in response. This suggests that our estimates of surround inhibition are well constrained. We conclude that centre–surround organisation is a generic property of the receptive fields of marmoset RGCs, as expected.

Synaptic inputs to marmoset RGCs

We now characterise the spatial tuning of excitatory and inhibitory synaptic inputs to RGCs, measured using whole-cell recordings from RGCs. Because different RGCs show different patterns of synaptic input, we first outline the synaptic inputs studied here. The left panels in Fig. 2*A*–*C* show total synaptic conductance during presentation of a light spot to an ON-RGC (Fig. 2*A*), or during presentation of a dark spot to two OFF-RGCs (Fig. 2*B* and *C*). Using standard techniques we decomposed the total conductance into excitatory and inhibitory synaptic conductances (see Methods), and these are shown in the middle and right panels of Fig. 2. As expected a light spot produced a large increase in excitation in every ON-RGC, and a dark spot produced a large increase in excitation in every OFF-RGC (Fig. 2*A*–*C*). Inhibitory conductance showed more diversity. A light spot of optimal size brought about a small increase in inhibition in 11/14 ON-RGCs (Fig. 2*A*), or no change in inhibition (3/14). On average, the magnitude of excitation was 2.77 ± 0.8 times that of inhibition for a spot of optimal size. In 5/24 OFF-RGCs a dark spot produced a small increase in inhibition (Fig. 2*B*; in these cells the magnitude of excitation was 3.83 ± 0.73 times greater than that of inhibition). In most (19/24) OFF-RGCs, however, a dark spot produced a large reduction in inhibition (Fig. 2*C*). In these RGCs the reduction in inhibitory conductance was similar to the increase in excitatory conductance (relative magnitude 0.99 ± 0.2). This pattern of response is similar to the disinhibitory mechanism described in alpha-like OFF-RGCs in other mammalian species, and from here on we will refer to it as disinhibition (Murphy & Rieke, 2006; Manookin *et al.* 2008; Van Wyk *et al.* 2009).

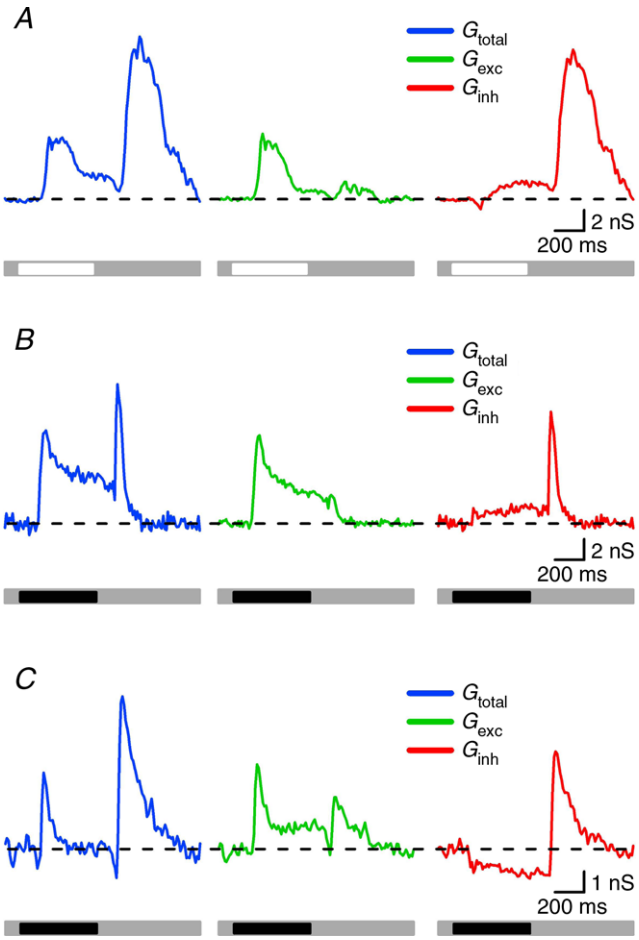

Figure 2. Synaptic conductance measurements for three RGCs in response to stimulation with an optimal size stimulus
A, representative synaptic conductance of an ON cell consisting of an increase in total conductance (blue trace) upon presentation and removal of a stimulus of preferred contrast. Excitation showed a large increase at stimulus onset and a small change at stimulus offset (green trace) and inhibition slightly developed at stimulus onset but greatly increased at stimulus termination (red trace). *B*, light-evoked conductances in an OFF-RGC that responded with increases in total membrane conductance at both phases of stimulus presentation (blue trace). Excitation showed a large increase at stimulus onset and a small increase at stimulus offset (green trace) whilst inhibition showed a mild but sustained increase at stimulus onset and a transient and large increase at stimulus offset (red trace). *C*, this OFF-RGC displayed increases in total conductance at both stimulus onset and offset (blue trace). Excitation was characterised by an increase at both stimulus phases (green trace) whilst the inhibitory conductance was reduced at stimulus onset (disinhibition) and showed a great increase at stimulus offset (red trace).

© 2013 The Authors. *The Journal of Physiology* published by John Wiley & Sons Ltd on behalf of The Physiological Society.

Downloaded from J Physiol (jp.physoc.org) at UCL Library Services on September 25, 2014

For completeness, Fig. 2 shows response at offset of the stimulus. Response at light offset was dominated by inhibition. In 9/14 ON-RGCs there was a large increase in inhibition at light offset. This was accompanied by a smaller increase in excitation (7/9 RGCs; Fig. 2*A*), or no change in excitation (2/9 RGCs). In 5/14 ON-RGCs light offset brought about no increase in either excitation or inhibition. Offset of the dark spot produced a large increase in inhibition in all OFF-RGCs. In 20/24 cells this was accompanied by a small increase in excitation. Excitatory synaptic inputs to both ON- and OFF-RGCs in marmoset are therefore largely drawn from bipolar cells of the same polarity (ON, OFF) as the RGC. In those ON- and OFF-RGCs where excitation can be recruited by stimuli of the non-preferred polarity, this increase in excitation is always much smaller than the associated increase in inhibition. We have not analysed the 'offset' conductances further. An additional two cells (2/40; 5%) showed ON–OFF responses when recorded extracellularly. These cells showed increases in total membrane conductance at both stimulus phases, with excitation being larger than inhibition at both phases (data not shown).

Spatial summation of synaptic inputs

Excitatory and inhibitory synaptic inputs onto the dendrites of RGCs originate in bipolar and amacrine cells, respectively. In addition, amacrine cells provide inhibition onto bipolar terminals (Cook & McReynolds, 1998; Flores-Herr *et al.* 2001; Eggers *et al.* 2007; Eggers & Lukasiewicz, 2010*a*). If the spatial profile of the amacrine cell receptive field is, however, no different from that of bipolar cells, the impact of amacrine cell input would be a change in overall sensitivity but no change in spatial summation. To assess whether spatial summation in amacrine and bipolar cells is similar, we compared spatial summation in inhibitory and excitatory synaptic inputs to RGCs. Figure 3 shows area–response functions of excitatory and inhibitory synaptic conductances: Fig. 3*A* shows the response of ON-RGCs, Fig. 3*B* shows the response of OFF-RGCs with disinhibition and Fig. 3*C* shows the response of OFF-RGCs with increased inhibition. The left panels in Fig. 3*A*–*C* show the spatial profile of excitatory and inhibitory conductances in example cells; the middle and right panels show average area–response functions for these conductances. In these cases we normalised response amplitude and size of each cell to the preferred stimulus before averaging; these average curves therefore disregard differences in spatial summation or response amplitude between cells. Figure 3 shows that excitatory and inhibitory conductance to ON- and OFF-RGCs show similar spatial summation on average. In the following we compare spatial summation in inhibitory and excitatory synaptic conductance. Our hypothesis is straightforward: if spatial summation of inhibition is no different from that of excitation, then this would indicate that inner retinal mechanisms have limited capacity to shape the spatial receptive field of RGCs. To characterise the area–response functions of individual RGCs we found the best predictions of a difference-of-Gaussians model of the receptive field (solid lines in Fig. 3). From these fits we extracted the spatial dimensions of the centre and surround for each conductance, and an index of spatial tuning (SI).

The centre radius of excitatory conductance was always less than 400 μm: for ON-RGCs it was 149 ± 43 μm, for OFF-RGCs with disinhibition it was 137 ± 22 μm and for OFF-RGCs with increase in inhibition it was 114 ± 30 μm. The centre radius of inhibitory conductance for ON-RGCs was 194 ± 44 μm, for OFF-RGCs with disinhibition 159 ± 28 and for OFF-RGCs with increase in inhibition 136 ± 21 μm. We investigated whether there was a consistent bias in the size of the inhibitory mechanisms among individual cells. This analysis showed that receptive field centre of inhibitory inputs was on average 120% the size of excitatory inputs ($P < 0.05$, $n = 35$). Among ON-RGCs this was 130% ($P < 0.05$, $n = 11$), for OFF-RGCs with disinhibition it was 116% ($P = 0.23$, $n = 19$) and for OFF-RGCs with inhibition 118% ($P = 0.23$, $n = 5$). We conclude that in general inhibitory conductance sums over slightly larger areas than excitatory conductance, and is therefore capable of modifying the spatial receptive field of RGCs.

Amacrine cell input would be more capable of modifying spatial tuning of RGCs if the spatial tuning of inhibition was different from that of excitation. We first quantified spatial tuning for excitation by comparing conductance during presentation of optimal (200–440 μm diameter) and large (1200 μm) spots of appropriate polarity. Figure 4*A* shows that in most cells (13/14 ON-RGCs; 21/24 OFF-RGCs), a large spot produced less excitation than an optimal spot, indicating centre–surround receptive field organisation in bipolar cell input to RGCs. To characterise the strength of the surround in each case, we calculated the proportional reduction in response as the stimulus was increased from optimal size to the largest tested. For excitation across all cell types this surround index (SI) was $43 \pm 5\%$ ($n = 38$). In ON-RGCs SI was $35 \pm 6\%$ ($n = 14$), in OFF-RGCs with disinhibition it was $48 \pm 9\%$ ($n = 19$) and in OFF-RGCs without disinhibition $47 \pm 11\%$ ($n = 5$). There was no significant difference in the SI of the three cell types ($P = 0.35$; ANOVA). These data confirm that the excitatory input to RGCs is spatially tuned.

Across the population of cells, the spatial tuning of inhibition was more variable than for excitation. Figure 4*B* shows that for some ON-RGCs (7/14) inhibition

© 2013 The Authors. *The Journal of Physiology* published by John Wiley & Sons Ltd on behalf of The Physiological Society.

Downloaded from J Physiol (jp.physoc.org) at UCL Library Services on September 25, 2014

was spatially tuned, confirming that the receptive field of inhibitory inputs to RGCs can show centre–surround organisation. For this subset of cells, SI was $59 \pm 6\%$ ($n = 7$). In other ON-RGCs (7/14), however, inhibition was no less for large spots than for small spots, or was substantially greater, indicating that in these cells inhibitory inputs do not show centre–surround organisation. In these cells inhibition for a spot of diameter 1200 μm was $190 \pm 80\%$ ($n = 7$) larger than for a spot of optimal diameter. Across all ON-RGCs a large stimulus increased inhibition at light onset on average by $65 \pm 54\%$ ($n = 14$; significantly different from that for excitation; $P < 0.05$). In OFF-RGCs, stimulation with a large spot in most cases reduced the magnitude of the inhibitory input. In those OFF-RGCs showing disinhibition, the SI for inhibition was $39 \pm 8\%$ ($n = 19$; not significantly different from that of excitation; $P = 0.25$), whilst in those OFF-RGCs displaying an increase in inhibition SI was $35 \pm 15\%$, not significantly different from that of excitation ($n = 5$; $P = 0.15$).

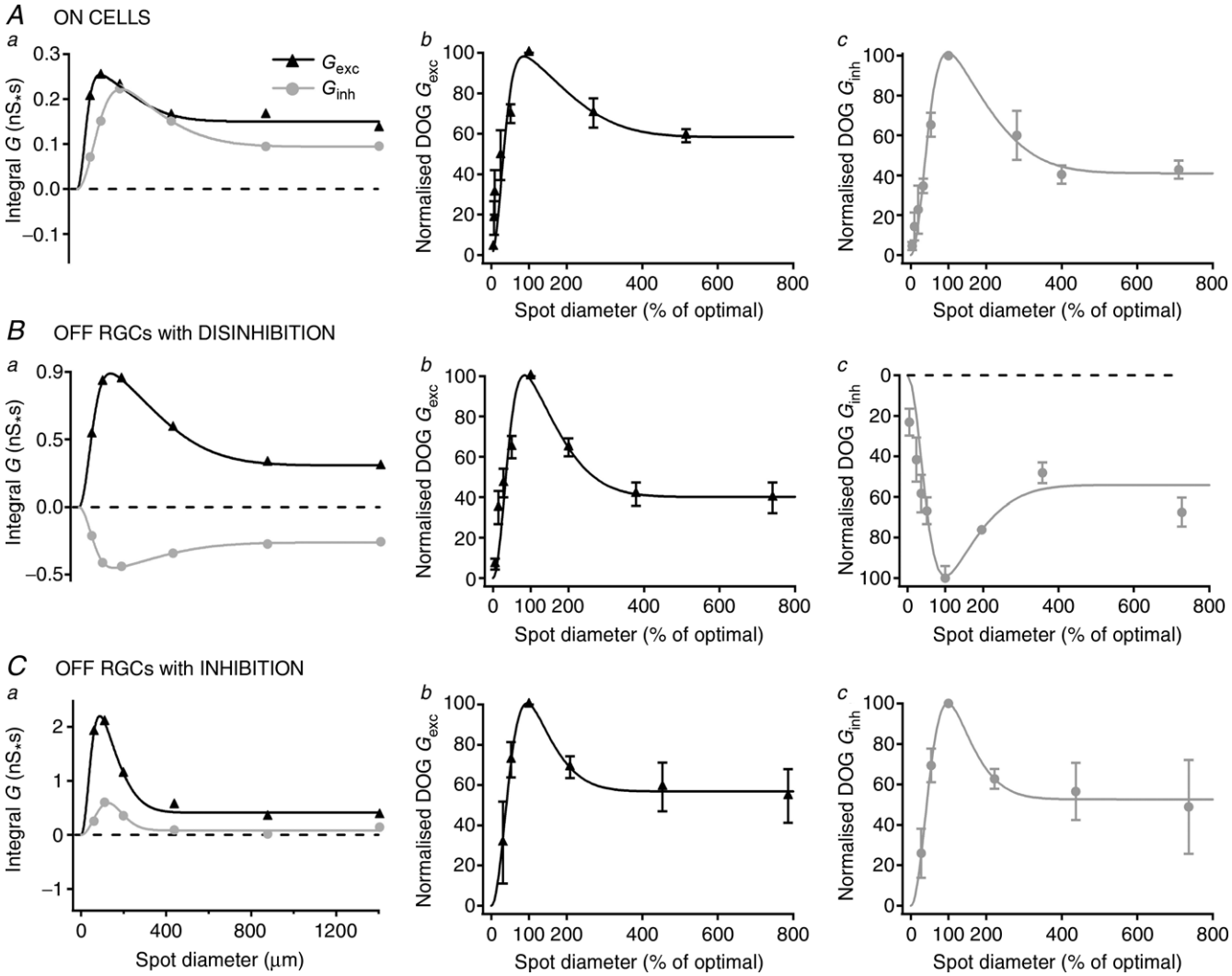

Figure 3. Area–response functions for excitatory and inhibitory conductances in ON cells and OFF cells with disinhibition and increase in inhibition

Area–response functions for excitatory and inhibitory conductances elicited by preferred stimulus in an ON cell (*Aa*), an OFF cell with disinhibition (*Ba*) and an OFF cell with increase in inhibition (*Ca*). The magnitude of excitatory and inhibitory synaptic inputs is expressed as the integral of their conductances. Symbols represent integral of conductance and solid lines show the best fit to a difference-of-Gaussian function. *Ab*, *Bb* and *Cb* show the average of the excitatory conductances normalised to optimal spot size and maximum response for 11 ON cells, 19 OFF cells with disinhibition and five OFF cells with increase in inhibition. *Ac*, *Bc* and *Cc* show the average of the inhibitory conductances normalised to optimal spot size and maximum response for 11 ON cells, 19 OFF cells with disinhibition and five OFF cells with increase in inhibition. Symbols are mean ± SEM and solid lines are the best fit to a difference-of-Gaussians function.

© 2013 The Authors. *The Journal of Physiology* published by John Wiley & Sons Ltd on behalf of The Physiological Society.

Downloaded from J Physiol (jp.physoc.org) at UCL Library Services on September 25, 2014

The analyses above show that both excitatory and inhibitory inputs to RGCs can show spatial tuning. Inhibition generally sums over larger areas of the retina than excitation, and show less spatial tuning than excitation. These observations suggest that, particularly for ON-RGCs, inhibition onto the RGC dendrites should contribute to spatial tuning in the RGC receptive field. There was substantial variability in the spatial tuning of the different synaptic inputs to individual RGCs, suggesting that they may draw differently on inhibitory inputs to shape the spatial receptive field.

Direct measurement of contribution of inner retinal inhibition to spatial tuning

Excitatory and inhibitory synaptic inputs onto the dendrites of RGCs originate in bipolar and amacrine cells, respectively. In addition, amacrine cells provide synapses onto bipolar terminals. Amacrine cells can therefore provide presynaptic inhibition, or postsynaptic inhibition, both of which may modulate the sensitivity and spatial profile of the receptive field of RGCs (Cook & McReynolds, 1998; Flores-Herr *et al.* 2001; Eggers *et al.* 2007; Eggers & Lukasiewicz, 2010*a*). The sodium channel blocker TTX has been used to identify the functional role of some of the amacrine cells that provide inner retinal inhibition, because it has a specific effect on those amacrine cells that propagate their signals via action potentials (Cook & McReynolds, 1998; Taylor, 1999; Flores-Herr *et al.* 2001; Shields & Lukasiewicz, 2003). Outer retinal neurons are not sensitive to TTX, and thus TTX selectively targets one of the potential sources of inner retinal inhibition. To determine whether these TTX-sensitive amacrine cells may contribute to the receptive field surrounds in primate RGCs, we first measured the effect of bath application of TTX on excitatory inputs to RGCs. In the following analyses we combined measurements from all RGCs, as the profile of excitatory conductance was similar in all of them.

Figure 5*A* shows excitatory currents from a ganglion cell, measured at the reversal potential of inhibition, during presentation of an optimal or large spot, in control conditions and in the presence of TTX. In control conditions responses to an optimal spot consisted of inward currents at both stimulus onset and stimulus offset. Presentation of a large spot reduced the inward current at stimulus onset to 22% of response to an optimal spot, and converted the inward current at stimulus offset into a small outward current. Addition of TTX to the bath increased the amplitude and duration of the response to an optimal spot at both stimulus phases, consistent with a removal of presynaptic inhibition at the level of bipolar cell terminals. For a large spot, TTX strongly increased response amplitude at stimulus onset, such that integrated response to a large spot was 99% that observed for what was an 'optimal' spot in control conditions. This is consistent with a strong suppression of presynaptic inhibition during application of TTX. In addition, responses to large spot stimuli under TTX revealed an inward current at stimulus offset, suggesting that it unmasked, or enhanced, an excitatory input by blocking presynaptic inhibition.

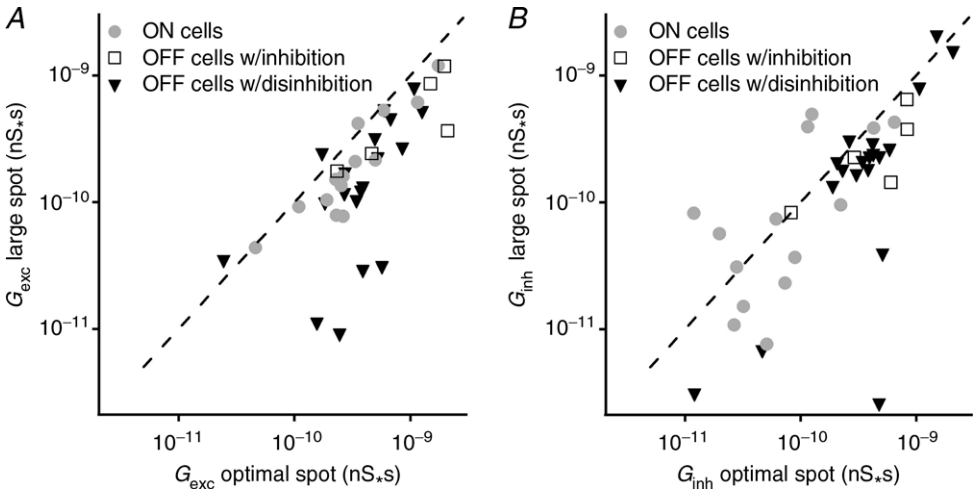

Figure 4. Surround stimulation in general reduces excitation and inhibition/disinhibition for all cell types
A, relationship between the magnitude of excitatory inputs elicited by spots of optimal and large size. *B*, relationship between the magnitude of inhibitory inputs elicited by spots of optimal and large size. The magnitude of excitatory and inhibitory synaptic inputs is expressed as the integral of their conductance and is represented by the symbols; the dashed line represents the line of unity.

© 2013 The Authors. *The Journal of Physiology* published by John Wiley & Sons Ltd on behalf of The Physiological Society.

Downloaded from J Physiol (jp.physoc.org) at UCL Library Services on September 25, 2014

Figure 5*B* shows the morphology of one RGC (left panel) and the area–response function of the excitatory currents onto it (right panel, filled symbols). The morphology of this cell is consistent with that of midget (parvocellular-pathway) ganglion cells in marmoset retina (Ghosh *et al.* 1996; Szmajda *et al.* 2008); the dendritic field diameter is 76 μm, similar to the diameter of the receptive field centre returned by fitting a difference-of-Gaussians

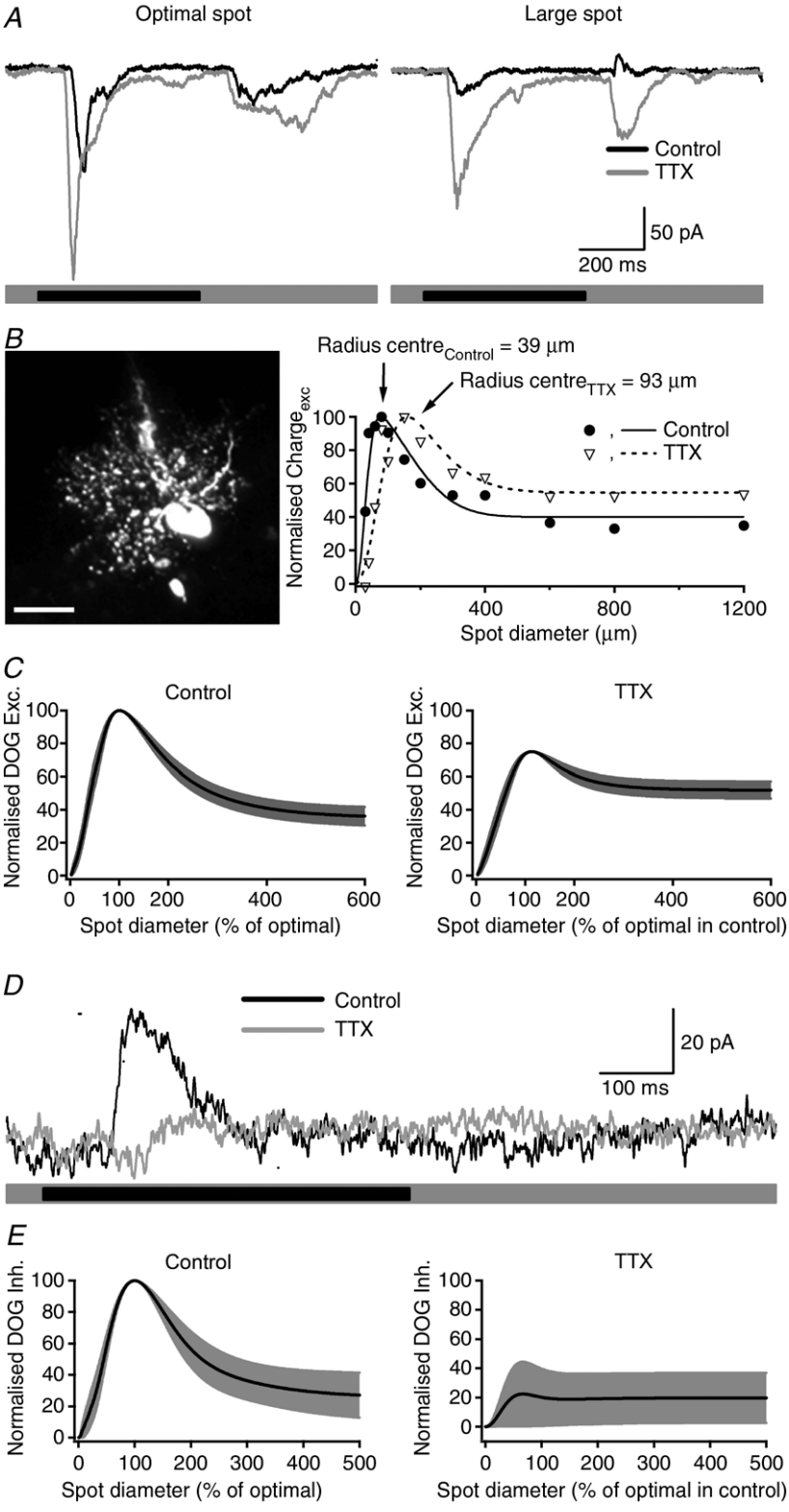

Figure 5. Effect of tetrodotoxin on excitatory input
A, excitatory input in the same OFF-RGC in response to centre stimulation is enhanced in the presence of TTX at both stimulus onset and offset. Stimulation of the surround reduces the central excitatory response in control conditions and TTX removes the suppressing effect of the surround stimulation. *B*, confocal stack of an ON-RGC filled with Lucifer Yellow and its corresponding area–response function of the excitatory current in control conditions and after bath application of 1 μM TTX. Filled circles and open triangles represent the excitatory charge transfer in control conditions and in the presence of TTX, respectively. Lines show the best fits to a difference-of-Gaussians function. TTX produced an increase of more than 2-fold in centre radius. Scale bar = 20 μm. *C*, average of area–response functions for excitatory currents normalised to optimal spot size and maximum current in control conditions and after bath application of TTX (n = 11 cells). Note that in the presence of TTX the roll off of the curve is less pronounced, indicating a lower degree of surround inhibition. *D*, inhibitory input onto RGCs elicited by annular stimulation consisted of outward currents at stimulus onset (black trace). Addition of TTX strongly reduced the inhibitory response (grey trace). The stimulus was a Dark annulus centred on the receptive field, inner diameter 150 μm and outer diameter 1400 μm. *E*, average of area–response functions for inhibitory currents normalised to optimal spot size and maximum current in control conditions and after bath application of TTX (n = 4 cells).

© 2013 The Authors. *The Journal of Physiology* published by John Wiley & Sons Ltd on behalf of The Physiological Society.

Downloaded from J Physiol (jp.physoc.org) at UCL Library Services on September 25, 2014

model to the area response for excitatory inputs (Fig. 5*B*; 78 μm). Figure 5*B* also shows area–response function for excitatory currents obtained during bath application of TTX (1 μM). In this RGC, TTX produced an expansion of the receptive field centre (diameter increased from 78 to 186 μm) and a reduction in the strength of the inhibitory surround: SI was reduced from 60% in control conditions to 44% during bath application of TTX.

We measured excitatory currents from 11 RGCs before and during bath application of TTX (excitatory inputs to ON- and OFF-RGCs were affected by TTX in the same way and we therefore do not distinguish them). Figure 5*C* characterises these measurements. The left panels in Fig. 5*C* show the best predictions of the difference-of-Gaussians model in control conditions, obtained independently for each cell. The right panels in Fig. 5*C* show similar curves, obtained during application of TTX. In each case we normalised response amplitude and size of each cell to the preferred stimulus in control conditions before averaging. Figure 5*C* shows that spatial tuning is less pronounced when the activity of spiking amacrine cells is abolished by bath application of TTX. On average, TTX had little impact on the receptive field centre. Radius increased from 108 ± 18 to 122 ± 11 μm, but this was not significant ($P = 0.17$). Sensitivity decreased, from 53 ± 10 to 40 ± 12, but this was not significant ($P = 0.11$). TTX had more of an impact on the receptive field surround. The radius of the surround was significantly reduced, from 333 ± 43 to 232 ± 37 μm ($P < 0.05$). The sensitivity of the surround was also reduced, from 42 ± 8 to 27 ± 10 ($P < 0.05$). The combination of these effects means that the volume of the surround was more strongly affected by TTX than the volume of the centre: the ratio of surround/centre volume decreased from 0.76 ± 0.06 to 0.54 ± 0.07 ($P < 0.01$). Similarly, TTX significantly reduced the SI from 65.1 ± 6.5 to 30.6 ± 7.8% ($P < 0.01$). The analyses above provide evidence that TTX-sensitive amacrine cells contribute to the receptive field surround present in the bipolar cell input to RGCs.

An additional mechanism by which inner plexiform interneurons can provide lateral inhibition is by directly inhibiting RGCs (Flores-Herr *et al.* 2001; Roska & Werblin, 2003). To determine if spiking amacrine cells may directly inhibit RGCs we measured the effects of bath application of TTX on inhibitory inputs to RGCs. For these measurements we restricted our analyses to RGCs that showed increased inhibition during presentation of a spot of preferred polarity (ON, OFF). For each of five cells, responses in control conditions consisted of outward currents. Figure 5*D* shows inhibitory currents from an OFF-RGC, during presentation of an annulus centred on the receptive field of the RGC, and measured at the reversal potential of excitatory currents. Annular stimulation was used to concentrate the measurements on mechanisms likely to be involved in the generation of the receptive field surround. TTX (1 μM) completely blocked inhibitory currents. We quantified the effect of TTX on the integral of the inhibitory currents (the stimulus-evoked charge transfer). TTX significantly reduced inhibitory input in all cells tested, reducing them to 23 ± 7% of control ($n = 5$; $P < 0.05$). This suggests that spiking amacrine cells can provide inner retinal inhibition directly to RGCs as well as to bipolar cells. Figure 5*E* shows the effect of TTX on the spatial tuning of inhibitory inputs, in the same format as Fig. 5*C*. Inhibitory inputs in control conditions were strongly tuned (right panel). TTX strongly reduced the strength of inhibition. The data in Fig. 5*D* and *E* suggest that TTX-sensitive inhibitory inputs have receptive fields that overlap the RGC dendritic field, and extend substantially beyond it.

Neurotransmitters providing direct inhibitory input

In non-primate mammals, inhibitory inputs to RGCs are mediated by GABA (Flores-Herr *et al.* 2001; Roska & Werblin, 2003) and glycine (Protti *et al.* 1997; Murphy & Rieke, 2006; Manookin *et al.* 2008; Van Wyk *et al.* 2009). To determine the contribution of GABAergic inhibition we measured currents while holding the membrane at the reversal potential for excitation, in control conditions and during bath application of the $GABA_A$ receptor antagonist SR 95531 (5 μM). Figure 6*A* shows the response of an ON-RGC during presentation of an annulus centred on the receptive field of the RGC. Responses in control conditions consisted of strong outward currents, which were completely abolished after addition of SR 95531 to the bath medium. As above, we made these measurements in cells that showed increases in inhibition at onset of the preferred stimulus. Across four cells SR 95531 reduced the charge transfer from 1.5 ± 0.8 to -0.2 ± 0.1 nS.s ($n = 4$; 2 ON cells, 2 OFF cells). Note the change in sign of the charge transfer, which indicates that in the presence of SR 95531 annular stimulation elicits small inward currents rather than outward currents. Figure 6*B* shows the morphology of the cell shown in Fig. 6*A*, and the area–response function for inhibitory currents, as measured with spots of light. The morphology of this cell is consistent with that of the narrow thorny ganglion cells in marmoset and macaque retina (Dacey *et al.* 2003; Ivanova *et al.* 2010). The dendritic field diameter of 274 μm is similar to the diameter of the inhibitory receptive field centre obtained by fitting a difference-of-Gaussians model to the receptive field (290 μm). During bath application of SR 95531 the area–response function for inhibition is flat and lies below zero, indicating the complete blockade of inhibitory inputs at all spot sizes. Figure 6*C* shows average spatial tuning of inhibitory inputs for three cells, in the same format as Fig. 5*C* and *E*; in these three cells inhibitory inputs were weakly tuned. SR 95531 obliterates direct inhibitory inputs at all stimulus sizes.

© 2013 The Authors. *The Journal of Physiology* published by John Wiley & Sons Ltd on behalf of The Physiological Society.

Downloaded from J Physiol (jp.physoc.org) at UCL Library Services on September 25, 2014

The results in Fig. 6 confirm that in cells with an increase in inhibition at stimulus onset, most or all of that inhibition is mediated by GABA, and arises from amacrine cells whose receptive fields overlap the RGC dendritic field, and extend substantially beyond it. The effect of the glycine receptor blocker strychnine was tested in two OFF-RGCs that showed disinhibition at stimulus onset. Strychnine decreased the tonic inhibitory input, strongly reduced the magnitude of disinhibition and increased the magnitude of the excitatory input (data not shown). This suggests that the synaptic mechanisms that provide disinhibition in primate retina are similar to those described in alpha-like RGCs of guinea pig and mouse.

Functional impact of inhibition

The analyses above show that inner retinal inhibition provides part of the receptive field surround of bipolar cells. These measurements do not, however, show how this inhibition shapes RGC receptive fields. In the following we use dynamic-clamp experiments to explore how TTX-induced changes in spatial tuning of excitation are reflected in the spatial tuning of the spike response of RGCs. For these experiments we first recorded area–response curves for excitatory and inhibitory conductances from an OFF-RGC that showed increases in excitation and inhibition at stimulus onset. We took measurements from that cell in control conditions and in the presence of TTX. The SI of the excitatory conductance in control conditions was 61%, and in the presence of TTX was 31%, in agreement with the results shown in Fig. 5. The decrease in SI of the excitatory conductance in the presence of TTX reflects the broader spatial tuning of inhibition. We then injected combinations of the recorded conductances into different RGCs. These experiments were made in the absence of any pharmacological agents, in light-adapted conditions. We first measured responses during injection of excitatory conductance and inhibitory conductance that had both been recorded in control conditions. Figure 7*A* (left panel) shows that injection of excitation and inhibition recorded during presentation of an optimal spot generated a robust spike response. Spike response was reduced when we injected conductances that were recorded during presentation of a large spot (Fig. 7*A*, right panel). This is consistent with a classical centre–surround organisation of the receptive field. We then measured responses during injection of excitation that had been recorded in the

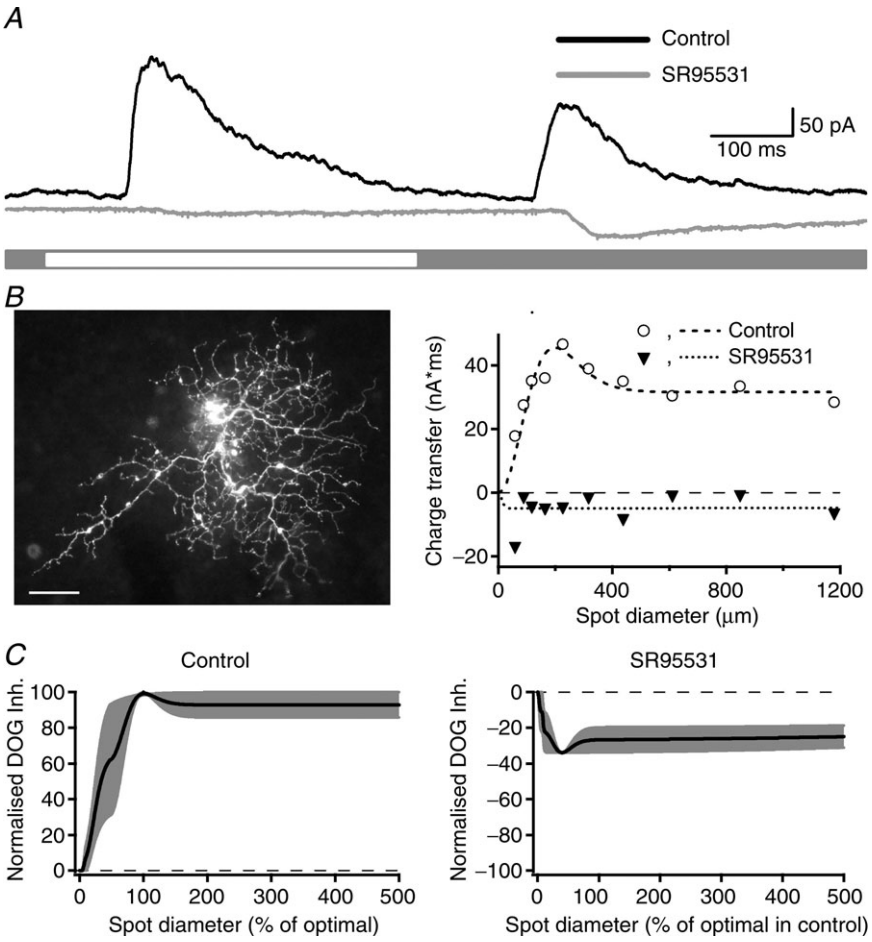

Figure 6. Effects of SR 95531 on direct inhibitory input in RGCs displaying increase in inhibition
A, light-evoked direct inhibitory input elicited by annular stimulation in an ON-RGC consisted of outward currents at both stimulus phases. These currents were abolished by SR 95531 (5 μM) and a small inward current was unmasked at stimulus onset and offset. *B*, morphology and area–response function of the inhibitory currents for the cell shown in *A* in control conditions and during bath application of SR 95531. *C*, average of area–response functions for inhibitory currents normalised to optimal spot size and maximum current in control conditions and after bath application of SR 95531 ($n = 3$ cells). SR 95531 completely abolished the direct inhibitory input onto RGCs for all stimulus sizes.

© 2013 The Authors. *The Journal of Physiology* published by John Wiley & Sons Ltd on behalf of The Physiological Society.

Downloaded from J Physiol (jp.physoc.org) at UCL Library Services on September 25, 2014

presence of TTX, and inhibition recorded in control conditions. Thus, this experimental paradigm mimics the effect of removing TTX-mediated inhibition onto bipolar cells, which is stronger for large spot diameters. Figure 7*B* shows the response to these conductances: responses to injection of conductance waveforms measured with an optimal spot were slightly increased (Fig. 7*B*, left panel) and responses to injection of conductance waveforms measured with large spots were strongly enhanced (Fig. 7*B*, right panel).

Figure 8 shows area–response functions for spike count during injection of the two combinations of conductances. Figure 8*A* shows average response, normalised to the maximum obtained in the control condition. Removal of TTX-mediated inhibitory input onto bipolar cells slightly reduced spike count for small sizes and significantly increased spike count for the largest sizes. To emphasise the impact of TTX on the receptive field surround we normalised the area–response function for each cell to its peak before averaging (Fig. 8*B*). The area–response function generated by control conductances shows the typical roll off at large sizes that is associated with the presence of a receptive field surround. The area–response function generated with mixed conductances shows less roll-off, consistent with a weaker receptive field surround. Figure 8*C* shows the percentage change in response as a function of stimulus size, and confirms that removal of TTX-mediated presynaptic inhibition has a stronger impact for larger stimuli, which engage the receptive field surround. To further quantify this roll-off we calculated the SI. Large SI observed during injections of control conductances (SI = 81 ± 5%) was halved when excitation recorded in the presence of TTX was co-injected with control inhibition (SI = 46 ± 5%; $n = 9$ cells, $P < 0.01$, Wilcoxon matched-pairs test). Taken together these results indicate that bipolar cells receive inhibitory inputs from spiking amacrine cells, and that these inhibitory inputs shape the receptive field surround of RGCs.

Discussion

The results above show a clear role for inner retinal inhibition in shaping the spatial profile of ganglion cell

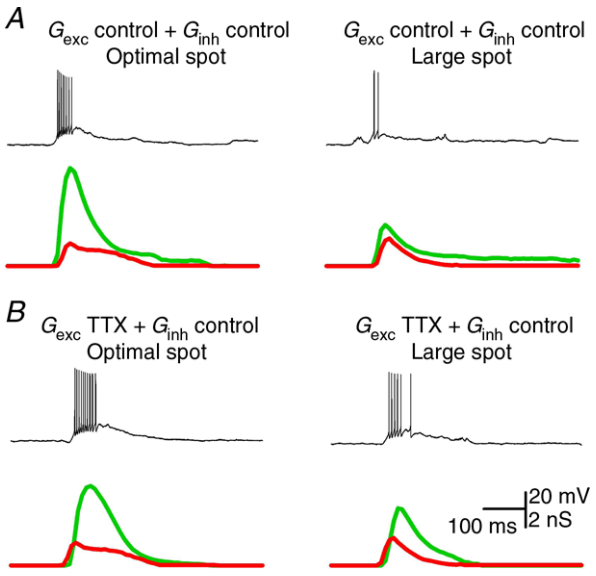

Figure 7. Modulation of excitatory inputs by TTX-mediated inhibition shapes receptive fields
A, action potentials evoked by somatic injection of control excitation (green) and inhibition (red) recorded in response to stimulation of the receptive field centre (left) and receptive field centre together with the surround (right). *B*, action potentials evoked by injection of control excitation (green) and inhibition recorded in the presence of TTX (red) when stimulating the receptive field centre (left) and the centre and surround areas (right).

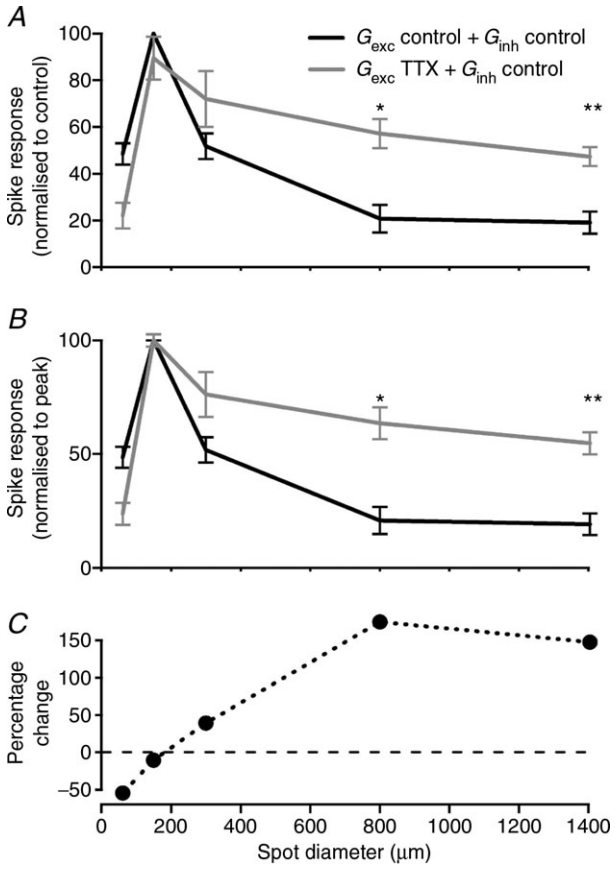

Figure 8. Quantification of the effect of removing TTX-mediated inhibition on bipolar cells
Average area–response functions: bottom curves show responses normalised to their own peak response in response to control excitation and inhibition (black) and in response to injection of control excitation and inhibition recorded under TTX (grey). Note the reduction in surround inhibition. Top curves show responses normalised to the peak response elicited by injection of control excitation and inhibition (black). Note the overall increase in response strength in addition to the reduction in surround inhibition (grey trace). $n = 9$ cells; $^*P < 0.05$; $^{**}P < 0.01$.

© 2013 The Authors. *The Journal of Physiology* published by John Wiley & Sons Ltd on behalf of The Physiological Society.

Downloaded from J Physiol (jp.physoc.org) at UCL Library Services on September 25, 2014

receptive fields in primate. First, blockade of inner retinal inhibition reduced spatial tuning in the excitatory inputs to ganglion cells. Dynamic-clamp recordings confirmed that TTX-mediated inhibition onto bipolar cells helps shape the spatial tuning of spike output. Secondly, direct inhibitory inputs to ganglion cells showed on average less spatial tuning than the excitatory input. Where inhibitory inputs are less spatially tuned they will be relatively stronger during presentation of a large stimulus, and this will further increase spatial tuning of ganglion cell spike output.

Spatial tuning of spike response and synaptic inputs

Recordings of spike response showed that the majority of RGCs exhibited centre–surround organisation of their receptive field. The average ratio of surround to centre volume measured in this study for ON- and OFF-RGCs was 0.58, similar to that reported for RGCs of the macaque retina, and for lateral geniculate nucleus cells in macaque and marmoset (Croner & Kaplan, 1995; Solomon *et al.* 2006; Alitto & Usrey, 2008, Cheong *et al.* 2013). Croner and Kaplan (1995) report that the size of the surround, relative to that of the centre, is 6.7 and 4.8 in parvocellular and magnocellular cells respectively. These are comparable to our average value for ON- and OFF-RGCs (4.1).

In most cells, stimulus-evoked synaptic inputs comprised a change in both excitation and inhibition/disinhibition. For those neurons where the onset of an optimal stimulus increased both excitation and inhibition, the excitatory input was always greater than the inhibitory input and at stimulus offset the change in inhibition was generally larger than in excitation. In OFF cells with disinhibition at stimulus onset, excitation was sometimes stronger than disinhibition, and sometimes weaker. Thus, some cells might be more sensitive to disinhibition than excitation. Making the stimulus larger reliably reduced the difference between excitation and inhibition (or disinhibition), so inhibition to primate RGCs is relatively stronger when the stimulus is large.

The 'centre' sizes of excitatory and inhibitory inputs were on average similar but we saw little correlation between the size of excitatory and inhibitory inputs in any cell class. Similarly, both excitatory and inhibitory inputs were usually spatially tuned but there was little correlation in the strength of surround inhibition of excitatory and inhibitory inputs. These results show that the spatial properties of inhibitory inputs are not simply related to those of the excitatory inputs and suggest that amacrine cell circuits may pool over more or different bipolar cell classes, with variability supplied by the coverage of bipolar terminals, their convergence onto amacrine cells or the degree of coupling of the amacrine cell network. For OFF-RGCs showing disinhibition, the lack of correlation in spatial tuning of excitation and disinhibition may further reflect the fact that excitation originates from the OFF pathway whilst inhibition arises in the ON pathway (Murphy & Rieke, 2006; Manookin *et al.* 2008; Munch *et al.* 2009; Van Wyk *et al.* 2009).

One possibility is that inhibitory inputs from amacrine cells onto bipolar cell terminals and onto ganglion cell dendrites are mediated by receptors with different sensitivity, or that receptor distribution varies in different receptive field areas, thus producing unequal impact on excitatory and inhibitory responses. Our measurements, however, are drawn from several ganglion cell classes and thus greater correlation might be identified if measurements were restricted to the same functional class (e.g. parasol or midget cells).

Impact of inner retinal inhibition on spatial tuning of RGCs

In the retina of lower vertebrates and non-primate mammals, inhibitory amacrine cells shape the output of bipolar cell terminals via GABA and/or glycine (Flores-Herr *et al.* 2001; Shields & Lukasiewicz, 2003; Vigh *et al.* 2011). We have shown here in the primate retina that spatial tuning of excitatory inputs is reduced during application of TTX: TTX reduces the size and volume of the surround of the receptive field of excitatory input. The most parsimonious explanation is that spiking amacrine cells in the IPL provide inhibitory input onto bipolar cell terminals, and through this provide a component of the classical surround, consistent with previous findings in the rabbit and mouse retina (Taylor, 1999; Flores-Herr *et al.* 2001; Zhang *et al.* 2012).

While TTX had no overall effect on the magnitude of excitatory inputs from bipolar cells, there was some inter-neuronal variability: TTX reduced the peak magnitude of excitatory currents in 8/11 RGCs and increased it in the other three. Increased magnitude of excitatory inputs, as with reduced spatial tuning, may reflect removal of inhibition onto bipolar cell terminals (Flores-Herr *et al.* 2001). Reduced excitatory currents may be explained if a subpopulation of bipolar cells in the marmoset retina use action potentials to boost their signals, as reported for bipolar cells in the ground squirrel and rat (Ma *et al.* 2005; Saszik & DeVries, 2012). Alternatively, a reduction in excitatory currents may reflect serial inhibitory processes, such that amacrine cells providing input to the bipolar cell terminals are themselves under the control of TTX-sensitive inhibition.

In addition, TTX reduced inhibitory inputs onto RGCs themselves, indicating that spiking amacrine cells may contribute to spatial tuning and response strength of RGCs by direct inhibition. TTX blocked annulus-evoked inhibitory inputs onto ganglion cells: this suggests that a component of TTX-sensitive inhibition must be mediated by active propagation within medium- or wide-field

© 2013 The Authors. *The Journal of Physiology* published by John Wiley & Sons Ltd on behalf of The Physiological Society.

Downloaded from J Physiol (jp.physoc.org) at UCL Library Services on September 25, 2014

amacrine cells, as previously shown for the rabbit retina (Bloomfield, 1996). In most cells, however, TTX also reduced the inhibition recruited by small spot sizes. This inhibition may arise from narrow-field amacrine cells that fire action potentials (Boos *et al.* 1993; Heflin & Cook, 2007). It might also arise from local subregions of the dendritic tree of wide-field amacrine cells. This type of local inhibition has been shown to be facilitated by TTX-dependent spikes within amacrine cells (Miller *et al.* 2006), and would therefore be reduced during bath application of TTX.

Direct inhibitory inputs onto RGCs are mediated by GABA and/or glycine (Protti *et al.* 1997; Tian *et al.* 1998; Van Wyk *et al.* 2009). GABAergic inputs are thought to arise from medium to wide-field spiking amacrine cells whilst glycinergic inputs are thought to originate from narrow-field amacrine cells (Protti *et al.* 1997; Zhang & McCall, 2012). Our results show that in those ON- and OFF-RGCs that show an increase in inhibition at the onset of a preferred stimulus, direct inhibitory inputs are almost completely blocked by a $GABA_A$ receptor antagonist. These results suggest that in the primate retina, direct inhibitory inputs will modulate the amplitude of spike output, as reported for several ganglion cell types in other species (Caldwell & Daw, 1978; Ariel & Daw, 1982; Ackert *et al.* 2006; de Vries *et al.* 2011).

Our results are consistent with reports in non-primate RGCs (Demb *et al.* 1999; Flores-Herr *et al.* 2001; Roska & Werblin, 2003). Previous work in ON parasol cells of macaque retina (McMahon *et al.* 2004) shows that picrotoxin attenuates annulus-induced membrane-hyperpolarisation. This is consistent with our measurements, which show that annuli recruit GABAergic input to ON-RGCs. Some of our results are, however, in contrast to the findings of McMahon *et al.* (2004), who did not find an effect of TTX on the spatial tuning of parasol cells in the macaque retina. The reason for this discrepancy is not clear. First, it might be due to differences among different cell types, although TTX showed a consistent effect in all cells we recorded from. Second, we measured synaptic currents using voltage-clamp, while McMahon *et al.* (2004) measured membrane potential using current clamp. Measurements of membrane potential cannot separate excitatory currents and inhibitory currents, so proportional changes in both may be invisible. Both our measurements and those of McMahon *et al.* (2004) show that bath application of TTX reduces excitation for small spots. In addition, our measurements show an increase in excitation for large spots, presumably because TTX reduces surround inhibition onto bipolar cell terminals. If membrane potential of the ganglion cell were modulated by excitation alone, then TTX would substantially reduce the strength of the surround. Bath application of TTX, however, also brought about a profound reduction in inhibition to the ganglion cell, and this reduction was most pronounced for small spot sizes. These concurrent changes in both excitation and inhibition may largely cancel, leading to little net change in membrane potential measurements. Third, our measurements were made under mesopic light levels while those of McMahon *et al.* (2004) were made under high-photopic light levels. A recent report in mouse rod bipolar cells shows that GABA and glycine mediate IPL inhibition at low light levels whilst excitatory amino acid transporters (EAATs) mediate inhibition at high light levels (Ichinose & Lukasiewicz, 2012). If similar mechanisms operate in cone bipolar cells, then IPL-mediated surround inhibition may be mediated by neurotransmitters at mesopic light levels, as in our experiments. In contrast, at high photopic levels like those used by McMahon *et al.* (2004) and Davenport *et al.* (2008), surround inhibition may be dominated by mechanisms in the OPL, with additional contribution from EAAT-mediated IPL mechanisms.

Most OFF cells in our sample (19/24) showed disinhibition at the onset of a preferred stimulus. As we did not consistently recover their morphology, we do not know if they are all of the same class (e.g. parasol cells: Crook *et al.* 2011), or whether in the marmoset retina there are different types of OFF cells with disinhibitory mechanisms. In the two OFF cells tested strychnine blocked the disinhibitory response, consistent with observations in OFF alpha-like RGCs in guinea pig and mouse retina (Manookin *et al.* 2008; Münch *et al.* 2009; Van Wyk *et al.* 2009).

Spiking amacrine cells provide gain control and spatial tuning

Previous attempts to elucidate the contribution of inner plexiform circuits to the receptive field surround relied on quantifying the effect of TTX on the spatial tuning of excitatory inputs and on the magnitude of inhibitory inputs onto RGCs (Flores-Herr *et al.* 2001; Roska & Werblin, 2003; Zhang *et al.* 2012). In addition, dialysis of the intracellular milieu of RGCs with a high chloride-containing solution provided further evidence that direct inhibition onto RGCs may also shape their spatial tuning (Flores-Herr *et al.* 2001). These studies, however, could not assess the precise impact of removing inhibitory inputs from spiking amacrine cells onto bipolar cells and thus the contribution of inner plexiform inhibition to the centre–surround organisation remained unidentified. We used dynamic clamp recordings to selectively remove TTX-mediated inhibition onto bipolar cells, an approach that provides unequivocal evidence for the contribution of the IPL to presynaptic inhibition and its influence on the receptive field surround of RGCs. Our results show that presynaptic inhibition mediated by spiking amacrine cells helps sharpen the spatial tuning of RGCs and modulates the strength of their spike response.

© 2013 The Authors. *The Journal of Physiology* published by John Wiley & Sons Ltd on behalf of The Physiological Society.

Downloaded from J Physiol (jp.physoc.org) at UCL Library Services on September 25, 2014

To our knowledge, this is the first direct demonstration of a role for presynaptic inhibition in spatial tuning. Thus, we conclude that inhibitory mechanisms in the IPL of the primate retina modulate the spatial tuning of RGCs.

References

Ackert JM, Wu SH, Lee JC, Abrams J, Hu EH, Perlman I & Bloomfield SA (2006). Light-induced changes in spike synchronization between coupled ON direction selective ganglion cells in the mammalian retina. *J Neurosci* **26**, 4206–4215.

Alitto HJ & Usrey WM (2008). Origin and dynamics of extraclassical suppression in the lateral geniculate nucleus of the macaque monkey. *Neuron* **57**, 135–146.

Ariel M & Daw NW (1982). Pharmacological analysis of directionally sensitive rabbit retinal ganglion cells. *J Physiol* **324**, 161–185.

Bloomfield SA (1996). Effect of spike blockade on the receptive-field size of amacrine and ganglion cells in the rabbit retina. *J Neurophysiol* **75**, 1878–1893.

Boos R, Schneider H & Wassle H (1993). Voltage- and transmitter-gated currents of all-amacrine cells in a slice preparation of the rat retina. *J Neurosci* **13**, 2874–2888.

Borg-Graham LJ (2001). The computation of directional selectivity in the retina occurs presynaptic to the ganglion cell. *Nat Neurosci* **4**, 176–183.

Caldwell JH & Daw NW (1978). Effects of picrotoxin and strychnine on rabbit retinal ganglion cells: changes in centre surround receptive fields. *J Physiol* **276**, 299–310.

Camp AJ, Cheong SK, Tailby C & Solomon SG (2011). The impact of brief exposure to high contrast on the contrast response of neurons in primate lateral geniculate nucleus. *J Neurophysiol* **106**, 1310–1321.

Camp AJ, Tailby C & Solomon SG (2009). Adaptable mechanisms that regulate the contrast response of neurons in the primate lateral geniculate nucleus. *J Neurosci* **29**, 5009–5021.

Chen X, Hsueh H-A, Greenberg K & Werblin FS (2010). Three forms of spatial temporal feedforward inhibition are common to different ganglion cell types in rabbit retina. *J Neurophysiol* **103**, 2618–2632.

Cheong SK, Tailby C, Solomon SG & Martin PR (2013). Cortical-like receptive fields in the lateral geniculate nucleus of marmoset monkeys. *J Neurosci* **33**, 6864–6876.

Cook PB & McReynolds JS (1998). Lateral inhibition in the inner retina is important for spatial tuning of ganglion cells. *Nat Neurosci* **1**, 714–719.

Croner LJ & Kaplan E (1995). Receptive fields of P and M ganglion cells across the primate retina. *Vision Res* **35**, 7–24.

Crook JD, Davenport CM, Peterson BB, Packer OS, Detwiler PB & Dacey DM (2009). Parallel ON and OFF cone bipolar inputs establish spatially coextensive receptive field structure of blue-yellow ganglion cells in primate retina. *J Neurosci* **29**, 8372–8387.

Crook JD, Manookin MB, Packer OS & Dacey DM (2011). Horizontal cell feedback without cone type-selective inhibition mediates "red-green" color opponency in midget ganglion cells of the primate retina. *J Neurosci* **31**, 1762–1772.

Dacey DM, Peterson BB, Robinson FR & Gamlin PD (2003). Fireworks in the primate retina: *in vitro* photodynamics reveals diverse LGN-projecting ganglion cell types. *Neuron* **37**, 15–27.

Davenport CM, Detwiler PB & Dacey DM (2008). Effects of pH buffering on horizontal and ganglion cell light responses in primate retina: evidence for the proton hypothesis of surround formation. *J Neurosci* **28**, 456–464.

de Vries SEJ, Baccus SA & Meister M (2011). The projective field of a retinal amacrine cell. *J Neurosci* **31**, 8595–8604.

Demb JB, Haarsma L, Freed MA & Sterling P (1999). Functional circuitry of the retinal ganglion cell's nonlinear receptive field. *J Neurosci* **19**, 9756–9767.

Di Marco S, Nguyen VA, Bisti S & Protti DA (2009). Permanent functional reorganization of retinal circuits induced by early long-term visual deprivation. *J Neurosci* **29**, 13691–13701.

Drummond GB (2009). Reporting ethical matters in the *Journal of Physiology*: standards and advice. *J Physiol* **587**, 713–719.

Eggers ED & Lukasiewicz PD (2010*a*). Interneuron circuits tune inhibition in retinal bipolar cells. *J Neurophysiol* **103**, 25–37.

Eggers ED & Lukasiewicz PD (2010*b*). Multiple pathways of inhibition shape bipolar cell responses in the retina. *Vis Neurosci* **28**, 1–14.

Eggers ED, McCall MA & Lukasiewicz PD (2007). Presynaptic inhibition differentially shapes transmission in distinct circuits in the mouse retina. *J Physiol* **582**, 569–582.

Enroth-Cugell C & Robson J (1966). The contrast sensitivity of retinal ganglion cells of the cat. *J Physiol* **187**, 517–552.

Farrow K, Teixeira M, Szikra T, Viney TJ, Balint K, Yonehara K & Roska B (2013). Ambient illumination toggles a neuronal circuit switch in the retina and visual perception at cone threshold. *Neuron* **78**, 325–338.

Flores-Herr N, Protti DA & Wässle H (2001). Synaptic currents generating the inhibitory surround of ganglion cells in the mammalian retina. *J Neurosci* **21**, 4852–4863.

Ghosh KK, Goodchild AK, Sefton AE & Martin PR (1996). Morphology of retinal ganglion cells in a new world monkey, the marmoset *Callithrix jacchus*. *J Comp Neurol* **366**, 76–92.

Heflin SJ & Cook PB (2007). Narrow and wide field amacrine cells fire action potentials in response to depolarization and light stimulation. *Vis Neurosci* **24**, 197–206.

Ichinose T & Lukasiewicz PD (2012). The mode of retinal presynaptic inhibition switches with light intensity. *J Neurosci* **32**, 4360–4371.

Ivanova E, Hwang GS, Pan ZH & Troilo D (2010). Evaluation of AAV-mediated expression of Chop2-GFP in the marmoset retina. *Invest Ophthalmol Vis Sci* **51**, 5288–5296.

Kremers J & Weiss S (1997). Receptive field dimensions of lateral geniculate cells in the common marmoset (*Callithrix jacchus*). *Vision Res* **37**, 2171–2181.

Ma YP, Cui J & Pan ZH (2005). Heterogeneous expression of voltage-dependent Na^+ and K^+ channels in mammalian retinal bipolar cells. *Vis Neurosci* **22**, 119–133.

Manookin MB, Beaudoin DL, Ernst ZR, Flagel LJ & Demb JB (2008). Disinhibition combines with excitation to extend the operating range of the OFF visual pathway in daylight. *J Neurosci* **28**, 4136–4150.

© 2013 The Authors. *The Journal of Physiology* published by John Wiley & Sons Ltd on behalf of The Physiological Society.

Downloaded from J Physiol (jp.physoc.org) at UCL Library Services on September 25, 2014

McMahon MJ, Packer OS & Dacey DM (2004). The classical receptive field surround of primate parasol ganglion cells is mediated primarily by a non-GABAergic pathway. *J Neurosci* **24**, 3736–3745.
Miller RF, Staff NP & Velte TJ (2006). Form and function of ON-OFF amacrine cells in the amphibian retina. *J Neurophysiol* **95**, 3171–3190.
Münch TA, da Silveira RA, Siegert S, Viney TJ, Awatramani GB & Roska B (2009). Approach sensitivity in the retina processed by a multifunctional neural circuit. *Nat Neurosci* **12**, 1308–1316.
Murphy GJ & Rieke F (2006). Network variability limits stimulus-evoked spike timing precision in retinal ganglion cells. *Neuron* **52**, 511–524.
Protti DA, Gerschenfeld HM & Llano I (1997). GABAergic and glycinergic IPSCs in ganglion cells of rat retinal slices. *J Neurosci* **17**, 6075–6085.
Rodieck RW (1965). Quantitative analysis of cat retinal ganglion cell response to visual stimuli. *Vision Res* **5**, 583–601.
Roska B & Werblin F (2003). Rapid global shifts in natural scenes block spiking in specific ganglion cell types. *Nat Neurosci* **6**, 600–608.
Sagdullaev BT & McCall MA (2005). Stimulus size and intensity alter fundamental receptive-field properties of mouse retinal ganglion cells *in vivo*. *Vis Neurosci* **22**, 649–659.
Saszik S & DeVries SH (2012). A mammalian retinal bipolar cell uses both graded changes in membrane voltage and all-or-nothing Na^+ spikes to encode light. *J Neurosci* **32**, 297–307.
Shields CR & Lukasiewicz PD (2003). Spike-dependent GABA inputs to bipolar cell axon terminals contribute to lateral inhibition of retinal ganglion cells. *J Neurophysiol* **89**, 2449–2458.
Solomon SG, Lee BB & Sun H (2006). Suppressive surrounds and contrast gain in magnocellular-pathway retinal ganglion cells of macaque. *J Neurosci* **26**, 8715–8726.
Solomon SG, Tailby C, Cheong SK & Camp AJ (2010). Linear and nonlinear contributions to the visual sensitivity of neurons in primate lateral geniculate nucleus. *J Neurophysiol* **104**, 1884–1898.
Solomon SG, White AJ & Martin PR (1999). Temporal contrast sensitivity in the lateral geniculate nucleus of a New World monkey, the marmoset *Callithrix jacchus*. *J Physiol* **517**, 907–917.
Szmajda BA, Grunert U & Martin PR (2008). Retinal ganglion cell inputs to the koniocellular pathway. *J Comp Neurol* **510**, 251–268.
Taylor WR (1999). TTX attenuates surround inhibition in rabbit retinal ganglion cells. *Vis Neurosci* **16**, 285–290.
Taylor WR & Vaney DI (2002). Diverse synaptic mechanisms generate direction selectivity in the rabbit retina. *J Neurosci* **22**, 7712–7720.
Thoreson WB & Mangel SC (2012). Lateral interactions in the outer retina. *Prog Retin Eye Res* **31**, 407–441.
Tian N, Hwang TN & Copenhagen DR (1998). Analysis of excitatory and inhibitory spontaneous synaptic activity in mouse retinal ganglion cells. *J Neurophysiol* **80**, 1327–1340.
Van Wyk M, Wässle H & Taylor WR (2009). Receptive field properties of ON- and OFF-ganglion cells in the mouse retina. *Vis Neurosci* **26**, 297–308.
VanLeeuwen M, Fahrenfort I, Sjoerdsma T, Numan R & Kamermans M (2009). Lateral gain control in the outer retina leads to potentiation of center responses of retinal neurons. *J Neurosci* **29**, 6358–6366.
Vigh J, Vickers E & von Gersdorff H (2011). Light-evoked lateral GABAergic inhibition at single bipolar cell synaptic terminals is driven by distinct retinal microcircuits. *J Neurosci* **31**, 15884–15893.
Wässle H (2004). Parallel processing in the mammalian retina. *Nat Rev Neurosci* **5**, 747–757.
Werblin FS (1974). Control of retinal sensitivity: II. Lateral interactions at the outer plexiform layer. *J Gen Physiol* **63**, 62–87.
Zhang CHI & McCall MA (2012). Receptor targets of amacrine cells. *Vis Neurosci* **29**, 11–29.
Zhang Y, Kim I-J, Sanes JR & Meister M (2012). The most numerous ganglion cell type of the mouse retina is a selective feature detector. *Proc Natl Acad Sci U S A* **109**, 2391–2398.

Additional information

Competing interests

None declared.

Author contributions

Work was conducted in the laboratory of D.A.P. at the University of Sydney. D.A.P., S.D.M. and S.G.S. designed the experiments, D.A.P., S.DM., J.Y.H., C.R.V. and V.N. performed the experiments, D.A.P., J.Y.H., C.R.V. and S.G.S. analysed the data, and D.A.P. and S.G.S. drafted the manuscript and all authors approved the final version.

Funding

This work was supported by an Australian Research Council grant (DP0988227) to D.A.P. and S.G.S., a Rebecca Cooper foundation grant to D.A.P. and an Australian Postgraduate award scholarship to C.R.V.

Acknowledgements

We thank Prof. Ulrike Grünert for her help with cell morphology analyses and Terence Middleton for technical assistance with some of the experiments.

© 2013 The Authors. *The Journal of Physiology* published by John Wiley & Sons Ltd on behalf of The Physiological Society.

Downloaded from J Physiol (jp.physoc.org) at UCL Library Services on September 25, 2014